Desalination and Water Treatment
www.deswater.com

doi:10.5004/dwt.2019.23477

141 (2019) 171–186
February

Experimental and numerical study of the characteristics of thermal and nonthermal offset buoyant jets discharged into stagnant water

Hassan Alfaifi[a,b,*], Abdolmajid Mohammadian[a], Hossein Kheirkhah Gildeh[a], Amir Gharavi[a]

[a]*Department of Civil Engineering, University of Ottawa, 161 Louis Pasteur, Ottawa, Ontario, Canada K1N 6N5, Tel. +1 613 562 5682, email: halfa103@uOttawa.ca (H. Alfaifi), majid.mohammadian@uOttawa.ca (A. Mohammadian), h.kheirkhah.gil@gmail.com (H.K. Gildeh), amir.gharavi@uOttawa.ca (A. Gharavi)*
[b]*King Abdulaziz City for Science and Technology (KACST), P.O Box 6086, Riyadh, Saudi Arabia*

Received 14 July 2018; Accepted 16 November 2018

ABSTRACT

This paper evaluates the effect of receiving water conditions on offset buoyant jet behavior. Several experiments on the discharge of thermal and nonthermal horizontal buoyant offset jets into stagnant ambient water are conducted. Particle Image Velocimetry (PIV) is used to measure the time history of the jet velocity distribution. Various characteristics of the jet flow, such as the centerline jet trajectory, jet growth rate and jet velocity decay, are discussed. All comparative experiments are conducted with the same densimetric Froude numbers (Fr_d, ranging from 9.9 to 29.8) and density differences $\Delta\rho$, ranging from 5.1 to 17.41). The results show that the trajectories of thermal jets are not the same as those of nonthermal jets, which suggests that thermal jets travel farther than nonthermal jets. The experimental results were then compared to predictions of three Reynolds-averaged Navier-Stokes (RANS) turbulence models: the standard *k*-ε, realizable *k*-ε, and buoyancy-modified *k*-ε. The best prediction of the centerline jet trajectory was found to be obtained from realizable *k*-ε. The study results revealed that the source of buoyancy (salinity versus temperature for the same values of Fr_d and same $\Delta\rho$) affects the trajectory and mixing properties of the jet.

Keywords: Offset jet; Buoyancy; Salinity; Particle Image Velocimetry (PIV); Densimetric Froude number; Realizable k-ε

1. Introduction

In recent decades, seawater desalination systems have been considered the best option for providing drinkable water to the public in arid and semiarid countries. This method has created an increased demand for the planning and execution of new desalination plant projects. The largest multistage flash (MSF) desalination plant in the world is located in Saudi Arabia, which is producing 0.96 million m^3/d of the drinkable water and approximately 1.4 million m^3/d of the effluents that is usually discharged back, with high temperature and salinity, to the aquatic environments [1]. These effluents are usually disposed using submerged pipes. These pipes (outfalls) are located on the coast near the plants and thus creates a plume of pollutants (i.e., jet) that may affect the marine environment.

It is important to carefully study a jet's behavior and its environmental impact on water bodies close to the discharge point. Several studies have revealed that discharging these effluents has an adverse influence on the marine ecosystem, particularly in the near-field zone of the discharge [2–7]. Therefore, it is necessary to study the characteristics of the near-field mixing zone to prevent any adverse impacts caused by the outfall systems and to maintain the marine environment such that it remains clean and suitable for its inhabitants and usable as a sustainable source of drinking water for future generations.

*Corresponding author.

Although outfalls with offset jets are currently used in many offshore industrial plants (e.g., desalination plants), little research has been conducted on their mixing characteristics, especially for buoyant offset jets with both salinity and temperature variations. Differences between the characteristics of the jet and those of the receiving water body (e.g., density differences due to salinity or temperature) may also affect the jet and its mixing characteristics.

Most previous experimental and numerical studies dealing with single-port horizontal offset jets have focused on dense jets discharged into fresh water [8–17]. Some of these studies were performed using the PIV system, either alone or in combination with laser-induced fluorescence (LIF). As mentioned above, most existing experimental studies have focused on offset dense jets; On the other hand, offset buoyant jets have rarely been studied and require further investigation.

Rawn and Palmer [18] were the first researchers to attempt to investigate the mixing characteristics of horizontal offset jets discharged into seawater, and their study included 388 experimental observations of dilution at the surface for offset freshwater jets injected into water of higher density. Later, Michas and Papanicolaou [19] investigated horizontal round turbulent buoyant jets discharged into a homogeneous and calm ambient fluid and studied both jet-like and plume-like cases to cover a wide range of applications. The mixing and geometric characteristics, such as trajectories, were obtained with video imaging; the turbulence properties were measured with fast response thermistors, and the dilution factors were evaluated. They found that the flow exhibited jet-like behavior in the horizontal regime; moreover, the mean and turbulent temperature profiles became asymmetrical in the transition and the vertical regime.

Recently, the effect of density differences between two liquids was studied by Eleuchet al. [20], who conducted some laboratory experiments to evaluate the evolution of a pure water jet injected vertically downwards into water of higher density. The researchers' study focused on the effect of the flow rate and the difference in density between the jet and the surrounding salt water. The results showed that jet penetration depth was affected by the flow rate and was increased by increasing the flow rate. Moreover, the jet penetration depth increased significantly when the density difference between the two liquids was decreased.

All the previously mentioned studies were conducted experimentally. However, numerical simulations of buoyant offset jets are ongoing and require further investigation. A numerical investigation of a round jet discharged horizontally and continuing with sediment particles was carried out by Liu and Lam [21]. The authors applied large eddy simulation (LES) for the fluid phase comparison, while Lagrangian particle tracking was used to calculate the motion of the sediment particles.

As a result, recent experimental and analytical investigations of outfall systems have indicated that Fr_d is correlated to many flow characteristics and can therefore be considered an influential parameter as a function of density [22,23]. Therefore, the mixing characteristics of buoyant jets can be controlled and affected by changing this important parameter.

To the best of the authors' knowledge, most of the existing literature on turbulent (positively) buoyant jets focuses either on flow kinematic behavior or on the mixing characteristics of effluent discharge into freshwater (as a dense or buoyant jet). However, the effects of the properties of the receiving water, particularly water of high salinity, on the mixing and trajectory characteristics of jets have rarely been studied. Thus, this paper reports experimental and numerical investigations of the behaviors of thermal and nonthermal buoyant offset jets discharged into fresh and saline stagnant water. Fourteen thermal and nonthermal experiments were conducted using the PIV technique. The performance of various turbulence models was then tested using the open-source CFD code, open field operation and manipulation (OpenFOAM) [24]. Three Reynolds-averaged Navier-Stokes (RANS) turbulence models were examined in this study (i.e., the standard *k*-ε , realizable *k*-ε and buoyancy-modified *k*-ε models), and the results were compared with the experimental data.

This paper is organized as follows. Theoretical concepts such as dimensionless groups and density calculation are presented in Section 2. In Section 3, the experimental setup and procedures are described. The results of some experimental cases are shown and discussed in Section 4. Computational approach such as governing equations, numerical methods and boundary conditions are presented in Section 5, as well as the preliminary results of numerical simulations compared with the experimental results. Finally, some concluding remarks complete the study.

2. Theory

2.1. Dimensionless groups

Fig. 1 shows a schematic sketch of an offset positive round buoyant jet discharging horizontally into a stagnant water body (ambient velocity, $U_a = 0$). The discharge port (jet) has diameter D and is placed above a horizontal solid surface at a specific distance. The receiving water (ambient water) is an unstratified fluid with a constant density ρ_a. The jet has a discharge velocity of U_0 and density of ρ_0 (where $\rho_0 < \rho_a$). The streamwise coordinates of the jet and the centerline of mean velocity are denoted by s and U_m, respectively, and b denotes the jet half-width.

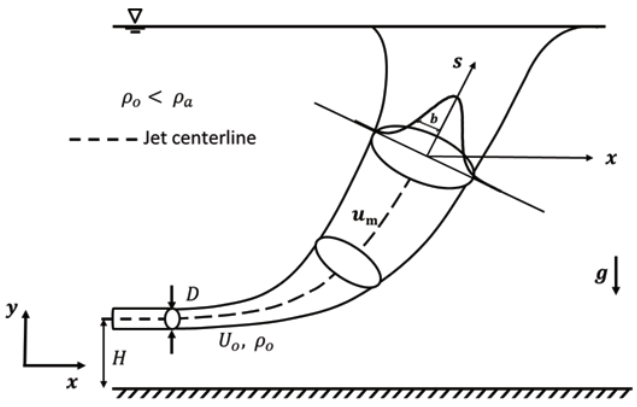

Fig. 1. Schematic sketch of a positive round buoyant jet in stagnant ambient water.

When a horizontal round buoyant jet is discharged into a stagnant fluid, the jet in the regions closer to the nozzle is dominated by momentum flux M_0 (i.e., within a short distance of the discharge port). The buoyancy flux effect B_0 then increases and dominates the jet, forcing it to rise to the water surface. Jet behavior is characterized by various fluxes: discharge volume flux $Q_0 = U_0\pi D^2/4$, momentum flux $M_0 = U_0 Q_0$, and buoyancy flux $B_0 = Q_0 g_0'$, where $g' = g(\rho_0 - \rho_a)/\rho_a$ is the effective gravitational acceleration and g is the gravitational acceleration [25]. L_M (the momentum length scale) is a measure of the distance over which the jet's momentum is more important than its buoyancy, and L_Q (the source length scale) indicates the length over which the source discharge is important. The axes are normalized using L_M where $L_M = M_0^{0.75}/B_0^{0.5}$ (the ratio of the momentum and buoyancy fluxes) and $L_Q = Q_0/M_0^{0.5}$ where (the ratio of the volume and momentum fluxes). To determine the geometric and mixing characteristics of the turbulent buoyant jet, these two length scales are used. The jet densimetric Froude number Fr_d, the ratio of inertia to buoyancy, can be derived for turbulent buoyant jets and is proportional to the ratio of length scales: $Fr_d = L_M/L_Q = U_0/(g'D)^{0.5}$. The mean velocity U_m of the jet centerline, which decreases with longitudinal distance s from the discharge point, can also be calculated using the formula as following [26]:

$$U_m = K\frac{\sqrt{M_0}}{s} \quad (1)$$

2.2. Density calculation

The density can be calculated based on the equation of state. Millero and Poisson's equation [27] is one of the most widely used formulas for calculating density as a function of temperature and salinity. This formula is referred to as the equation of state of seawater and is used in this paper for calculating the density. The limits of temperature and salinity in this equation are $0 < T < 40$, $0.5 < S < 43.0$. Later, Millero and Huang [28] conducted new seawater density measurements to modify Millero and Poisson's [27] equation of state with the aim of expanding its limits to a wider range of temperature (0–90°C) and absolute salinity S_A (0–70 kg/m^3) values and found that the results obtained were consistent: the standard error was 0.0063 kg/m^3.

3. Experimental setup and procedures

The scaled model experiments were conducted in the Water Resources Laboratory at the University of Ottawa, Canada. The experiments were performed in a rectangular transparent glass tank 1.2 m long, 0.5 m wide, and 0.5 m deep, as shown in Fig.2. The bottom and sidewalls of the tank were made of glass panels. A circular nozzle with an internal diameter of 5.18 mm was placed horizontally at one end of the tank (centered), far enough (10 cm) from both the bed and back walls to avoid any influences and to ensure a fully developed velocity profile. All experiments were performed using water from the same source (i.e., tap water). A buoyant jet (with a density less than that of the receiving water) was generated by discharging water (heated into cold water for thermal jets and unheated freshwater into dense water for nonthermal jets) into the tank through this nozzle.

The nozzle was connected to a pipe equipped with: (1) a flow meter (Rotameter, FL-3840ST, up to ±2% FS accuracy, OMEGA) to determine the flow rate of the discharged water; (2) valves to control the discharge water. The pipe was connected to a constant-head tank with dimensions of 0.75 m length, 0.3 m width, and 0.3 m depth. This tank (con-

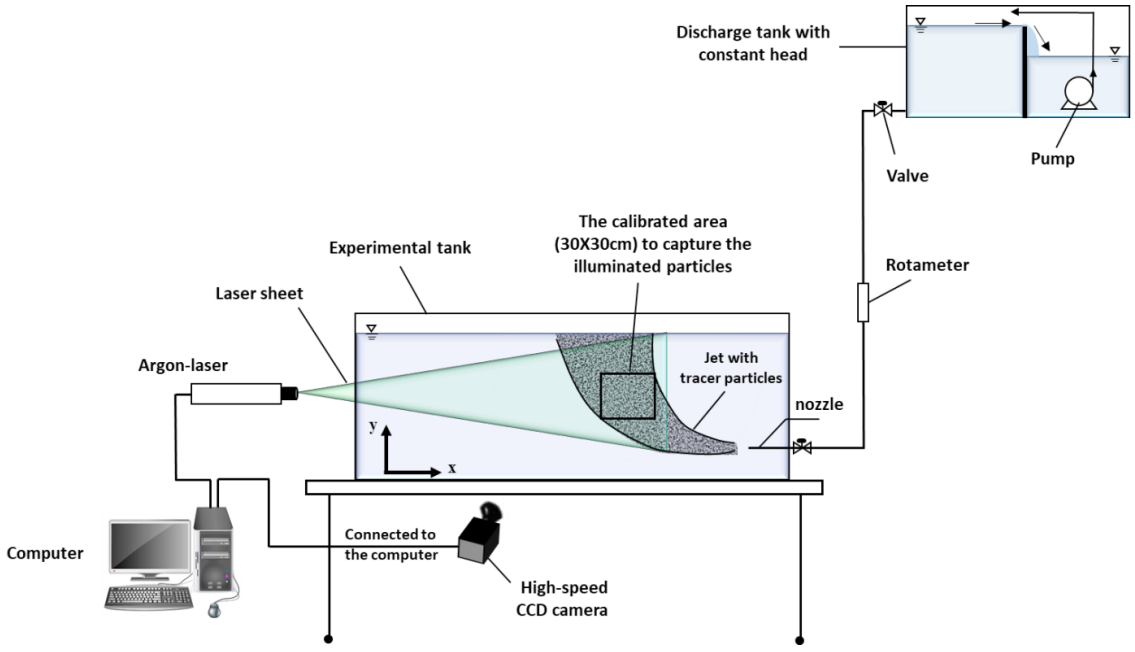

Fig. 2. Schematic view of the experimental setup with the PIV system.

taining the discharge water, which was fed by gravity into the large tank) was located approximately 1.5 m above the discharge nozzle.

The constant-head tank had two separate storage tanks, one of which was used to store surplus discharged water, as shown in Fig. 2. The water was then returned from the storage tank using a pump to maintain a constant water level. The storage tank was equipped with an instrument that enabled precise temperature control (Corio CD Heating Immersion & Bridge Mounted Circulator) with an accuracy of approximately ±0.03°C. This device was used to ensure that the temperature in the discharge tank remained constant during the experiments. To ensure that the water temperature in the pipe was equal to that of the heated water in the elevated tank, the pipe was covered with insulating material. Another outlet was located at the end of the discharged pipe, outside of the experimental tank, at a distance of 20 cm upstream of the nozzle tip to test the temperature of the discharged water before running the experiments. Moreover, the nozzle outlet was equipped with a very thin sensor, which was connected to a thermometer, to measure the flow temperature during the experiments.

3.1. Particle Image Velocimetry (PIV)

In the present study, a PIV system was used to measure the time history of the velocity distribution. PIV system is an experimental technique which has four main components: a laser box (a Nd:YAG laser with an energy level of 25 mJ per pulse), a laser lens, a high-speed camera (sCMOS), and a computer for synchronizing the camera and laser. The main function of the PIV system is to photographically record the movement of tracer particles in fluid. Thereafter, the motion of the particles is determined using image processing methods, and the flow velocity is obtained from the photographic recordings. In most applications, small tracer particles are added to the discharge flow to follow the fluid path. Two green laser beams were emitted from the laser box at a wavelength of 532 nm and were designed to overlap to ensure the correct velocity field calculation. The beams were then passed through the optical system to generate planar laser sheets. The high-resolution sCMOS camera (1008–1018 pixels) was placed at a cross-section of the tank that was illuminated by a laser sheet to capture the illuminated tracer particles in the fluid flow. An optical filter was placed in front of the camera lens to allow wavelengths of less than 532 nm, which were scattered by the particles, to pass. Images were recorded in the double-frame (image) mode; from these images, the instantaneous velocity field was calculated by cross-correlation calculations between the two frames. During laser illumination, the camera captured two frames (one frame for each pulse of the pulse pair) separated by a very small time interval. The obtained images were then transferred to the processor for the cross-correlation computations [29].

3.2. Experimental procedure

Two sets of experiments were conducted using a high-resolution camera to determine the jet behavior under two sets of conditions. The jet velocity was captured using the PIV system. The capture zone was a 30 cm × 30 cm square area of the jet trajectory, as shown in Fig. 2. In the first set of experiments, a thermal buoyant offset jet of hot water was discharged into cold water. The second set of experiments utilized a different concept to generate a buoyant jet without the presence of a temperature differential, in which a high concentration of salt (sodium chloride; NaCl; high purity (99.99%)) was dissolved in the ambient water to increase its density, while the discharged water was fresh (i.e., not saline). The temperatures of the jet and the ambient water were identical. The density was highly dependent on changes in salinity due to the similarity of the temperature in both fluids. For each comparison experiment, the values of Fr_d and $\Delta\rho$ were constant. The amount of salt required to achieve the target density difference was calculated using the Millero and Poisson [27] formula. The experimental parameters are summarized in Table 1.

In this study, two different concepts have been used in the two sets of experiments (fourteen experiments), which are divided into two groups. Each group has seven cases with the following features: In the first group (the first set of experiments, thermal experiments, i.e., T1 to T7), the density gradient is caused only by the difference in temperature, and the salinity is zero. In the second group (the second set of experiments, nonthermal experiments, i.e., S1 to S7), the density gradient arises from differences in salinity, and the domain temperature is constant. Two parameters were maintained at similar levels in all comparisons: the Fr_d and $\Delta\rho$ between the jet and ambient water.

To determine whether the source of the density difference (temperature versus salinity) affects jet behavior, as controlling parameter, the density differences due to temperature ($\Delta\rho_{thermal} = \rho_a - \rho_0$) and salinity ($\Delta\rho_{nonthermal} = \rho_a - \rho_0$) were also set as equal ($\Delta\rho_{thermal} = \Delta\rho_{nonthermal}$) in the two groups of experiments. In these experiments, the development of the jet was recorded using a PIV system. For brevity, only the results of three comparison cases (T1 and S1, T3 and S3, and T7 and S7) are shown in most of the figures.

4. Experimental results and discussion

4.1. Experimental observations

Finding the parameter with the most influence over jet flow characteristics and behavior is complicated since each parameter is influenced by others. For example, many flows are characterized by and correlated with a densimetric Froude number,which is considered a function of density. Moreover, the density of effluents can be changed by altering their temperature or concentration (here, salinity). Therefore, changing the density of the discharge water can also control the jet characteristics. Thus, it is logical to assume that jets with different temperatures and salinity values but with the same densimetric Froude number can behave similarly provided they are discharged into the same ambient water conditions. However, if the ambient water conditions are changed, the effect of these parameters may be expected to change, and the jet behavior would not be the same.

To further clarify this point, Fig. 3 shows the results for two cases of offset buoyant jets with the same densimetric Froude number and density difference ($\Delta\rho_{thermal} = \Delta\rho_{nonthermal}$). One can clearly see the difference in the jet trajectories; one

Table 1
Experimental parameters

Case	D	U_0	T_0	S_0	ρ_0	T_a	S_a	ρ_a	Fr_d	$\Delta\rho$
	(mm)	(m/s)	(°C)	(ppt)	(kg/m^3)	(°C)	(ppt)	(kg/m^3)		(kg/m^3)
Thermal jet experiments										
T1	5.18	0.16	38.6	0.0	992.75	21.5	0.0	997.89	9.9	5.1
T2	5.18	0.32	39.6	0.0	992.37	21.5	0.0	997.89	19.1	5.5
T3	5.18	0.23	50.5	0.0	988.06	21.5	0.0	997.89	10.3	9.8
T4	5.18	0.45	50.7	0.0	987.75	21.5	0.0	997.89	19.8	10.1
T5	5.18	0.48	39.55	0.0	992.39	22.2	0.0	997.73	29.1	5.3
T6	5.18	0.67	50.65	0.0	987.77	22.2	0.0	997.73	29.8	10.0
T7	5.18	0.60	66.4	0.0	980.24	23.3	0.0	997.47	20.25	17.23
Nonthermal jet experiments										
S1	5.18	0.16	21.5	0.0	997.89	21.5	6.79	1003.00	9.9	5.1
S2	5.18	0.32	21.5	0.0	997.91	21.4	7.33	1003.50	19.1	5.6
S3	5.18	0.23	21.3	0.0	997.93	21.3	13	1007.80	10.3	9.8
S4	5.18	0.45	21.3	0.0	997.95	21.2	13.52	1008.20	19.8	10.2
S5	5.18	0.48	21.3	0.0	997.91	21.4	6.80	1003.10	29.8	5.1
S6	5.18	0.67	21.2	0.0	997.97	21.1	13.3	1008.00	29.7	10.1
S7	5.18	0.60	34.5	0.0	994.21	34.5	23.6	1011.62	20.29	17.41

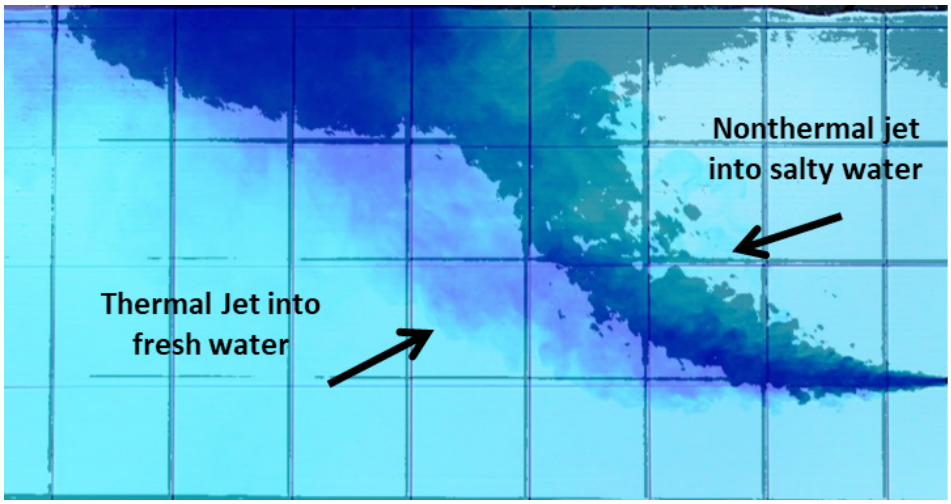

Fig. 3. Comparison between the jet trajectory patterns of thermal and nonthermal jets [30].

(nonthermal) jet reaches the water surface at a point closer to the source of discharge than the other. Therefore, to visualize the effects of the receiving water conditions on the jet trajectory of any discharged flow, numerous experiments have been conducted. In experiments in which salt was used in the ambient water (i.e., nonthermal experiments), all jets reached the water surface at shorter distance from the source than those reached in the thermal experiments. Moreover, the time to reach the surface was also shorter. More details are presented in the next section. In addition, the nonthermal jets reached the water surface with a higher velocity than was the case for the thermal jets. This result is evidence that a mechanism is making the jet rise faster toward the water surface. This raises an important point about this mechanism and its interaction with the momentum force: It is anticipated that nonthermal jets decay faster than thermal jets.

4.2. Jet evolution and propagation speed

When buoyant jets are discharged into two stagnant water bodies with different properties, the evolution and propagation of the jets may differ. To verify this notion, an experiment was conducted to compare thermal and nonthermal jets with similar densimetric Froude number and density differences as they discharged into tanks with different ambient water conditions: freshwater (zero salinity) and denser, saline water. A blue dye was used to visualize the

jet trajectories. It was observed that the penetration of the thermal jet was very slow; thus, it reached the surface more slowly than the nonthermal jet, which penetrated faster and reached the surface in less time and over a smaller distance. These phenomena and the times taken for both jets can be seen in Fig. 4.

From the thermal jet experimental results, it was observed that the jet penetrates the ambient water horizontally and progressively slows down. During this transient phase, a large head is formed in front of the jet. At a certain distance from the nozzle, the jet reaches a maximal depth of penetration, the buoyancy flux becomes larger, and the jet begins to slowly rise toward the water surface. Gradual expansion was observed from both sides of the thermal jet (inner and outer) from the nozzle to the extreme point of the jet prior to reaching the water surface. It is clear from

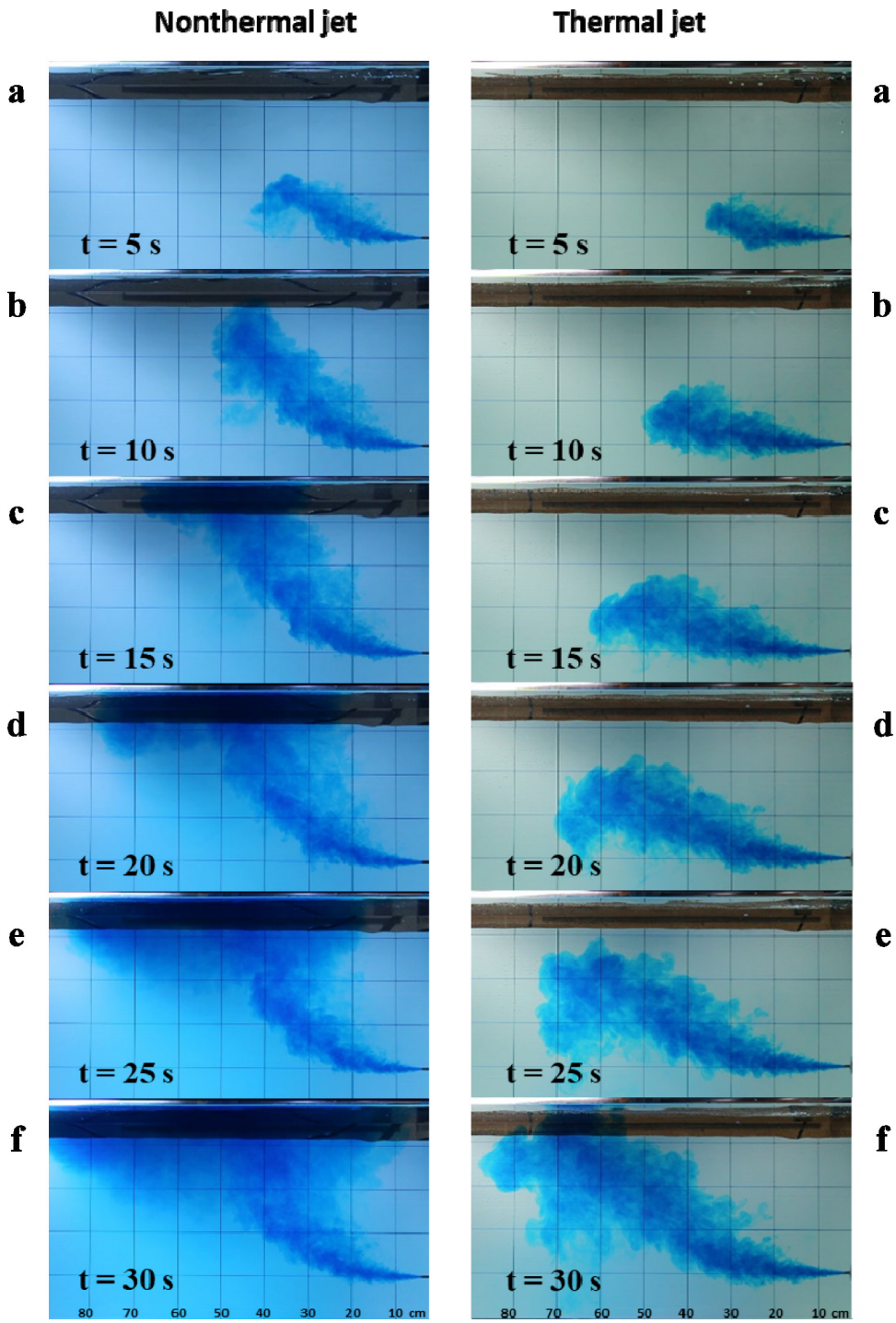

Fig. 4. Comparison between the times to reach the water surface for the thermal and nonthermal jets (cases T7 and S7).

the figures that the thermal jet propagates more slowly than the nonthermal jet. It can also be seen that the thermal jet reached the stationary depth (the point at which the effective force on the jet transforms from momentum to buoyancy flux) at t = 10 s, started to slowly rise to the top at t = 15 s, and reached the surface at t = 30 s. However, in the nonthermal case, the jet reached the stationary depth of penetration at less than 5 s and reached the surface at t = 12 s; that is, the thermal jet took three times longer to reach the water surface than the nonthermal jet.

Although the flow rate, Fr_d and Δρ were the same in both experiments, the jet penetration depths were different. The results were consistent with those obtained by Eleuch et al. [20], who demonstrated that jet penetration depth and head spread decrease as the difference in density between the jet and ambient water increases.

In contrast, in the nonthermal experiments, the jets were progressively faster, and no head development was seen. As clearly shown in the figures for the nonthermal jet (Figs. 4a–f), the jet reached the water surface at a distance of 40 cm in an axial direction from the nozzle tip; in contrast, the thermal jet took longer and reached the water surface at a distance of more than 70 cm. It was also noted that the effect of buoyancy on the nonthermal jet may have started earlier and at a shorter distance from the nozzle and then forced the jet to rise toward the water surface more rapidly. This distance is shorter than that in the case of the thermal jet. Moreover, to compare the propagation, consider Fig. 4a at 5 s for the nonthermal jet and Fig. 4c at 15 s for the thermal jet; it can be seen that the thermal jet is clearly wider.

This result may lead to the conclusion that if the jet remains longer within the water before reaching the surface, the jet propagation increases, thus increasing the dilution. These figures were chosen for comparison due to the similarity of the locations and distances from the nozzle. In addition, it was seen that the jet tends to be flatter before reaching the water surface for all thermal experiments than for the nonthermal cases, which are mostly steeper.

An explanation of these phenomena is as follows. The difference between the two cases might be attributed to the difference in the content of the ambient water, which can be considered a solution with physical properties for the thermal experiment and a solution with chemical properties for the nonthermal experiment. Indeed, in the thermal experiment, the jet can be affected by the surrounding cold water. Thus, the thermal energy of the jet is mainly lost in the surrounding water;hence,the jet's velocity decays more rapidly [31]. However, for the nonthermal experiment, it is known that if the water molecules are totally saturated with salt, it becomes a highly concentrated solution, such that there is less opportunity for any solution to move between the water molecules. Therefore, due to its low density, the solution rises up, after a distance, from the nozzle to the surface of the water.

As a result, when comparing the jet trajectories of the thermal and nonthermal cases, the divergence between the jets was noted to increase. Therefore, the density difference due to different salinity can be considered an influential parameter that can affect and change the jet trajectory. Thus, based on the results obtained in this study, it could be argued that salinity can also be considered a significant parameter for characterizing jet flow in a fluid.

4.3. Jet flow pattern

Dispersion of the fluid discharged within a water body can be affected by the characteristics and conditions of the receiving fluid. In this study, it was observed that the jet pattern required less time and distance to rise to the surface in the nonthermal experiments (retracted backward) than in the thermal experiments, in which the salinity in both the discharged and receiving water was zero. Fig. 5 presents superimposed time-averaged velocity vectors and contour maps of the velocity obtained from the PIV results for two comparison cases (T1 compared with S1, and T3 compared with S3); Fr_d was 9.9 for the first comparison and 19.8 for the second.

The PIV experimental results showed that all the nonthermal jets reached the water surface within a shorter distance than the thermal jets. In the thermal cases, the ambient water conditions (zero salinity) seem to allow the jet to spread more easily when compared with the nonthermal cases; this causes the jet to travel farther from the nozzle and reach the surface at a point farther than that reached by the nonthermal jet. As a result, the jet spread is greater for the thermal jet and increases gradually as the distance from the source increases, indicating greater dilution. This process was previously reported for a negatively buoyant jet (i.e., a dense jet) [32,33]. These authors mentioned that when the jet trajectory is longer, the dense jet can achieve a higher dilution; as a result, if the jet remains in the water body for a longer time before reaching the surface, the discharged water will become more diluted. Therefore, and based on the present study, it can be argued that if a thermal jet is discharged into stagnant and unstratified water, the level of dilution will be higher than for a nonthermal jet.

An industrial plant discharging cold freshwater that reaches the water surface at a point closer to the source is an example of a nonthermal jet. Therefore, this result is likely to be of importance in practical applications for avoiding the environmental impacts of outfall systems, as it relates to determining how far the intake pipe (feed pipe) should be placed from desalination plants.

4.4. Jet trajectory

Jet trajectory, also known as jet centerline, is a very important parameter in outfall system design because it identifies the path followed by the jet and the location where the jet reaches the water surface (in the case of a positive jet) or the seabed (in the case of a negative jet). The jet trajectory passes through three regions: 1) an initial region, 2) a transitional region, and 3) a buoyant or free-jet region. In this study, the results of both experiments were obtained at the transition region and at the beginning of the buoyant region. The centerlines of the mean velocities obtained from the experimental measurements of the thermal and nonthermal jets are shown in Fig. 6. The centerline values are obtained from the maximum velocity at various cross-sections of the jets. Three different experimental results obtained with different values of Fr_d and Δρ are shown for comparison. The Fr_d values were ≈ 10 for the first and second comparisons and ≈ 20 for the third comparison. The Δρ values were ≈ 5 for the first comparison and ≈ 10 for the second and the third comparisons. The results clearly indicate a difference

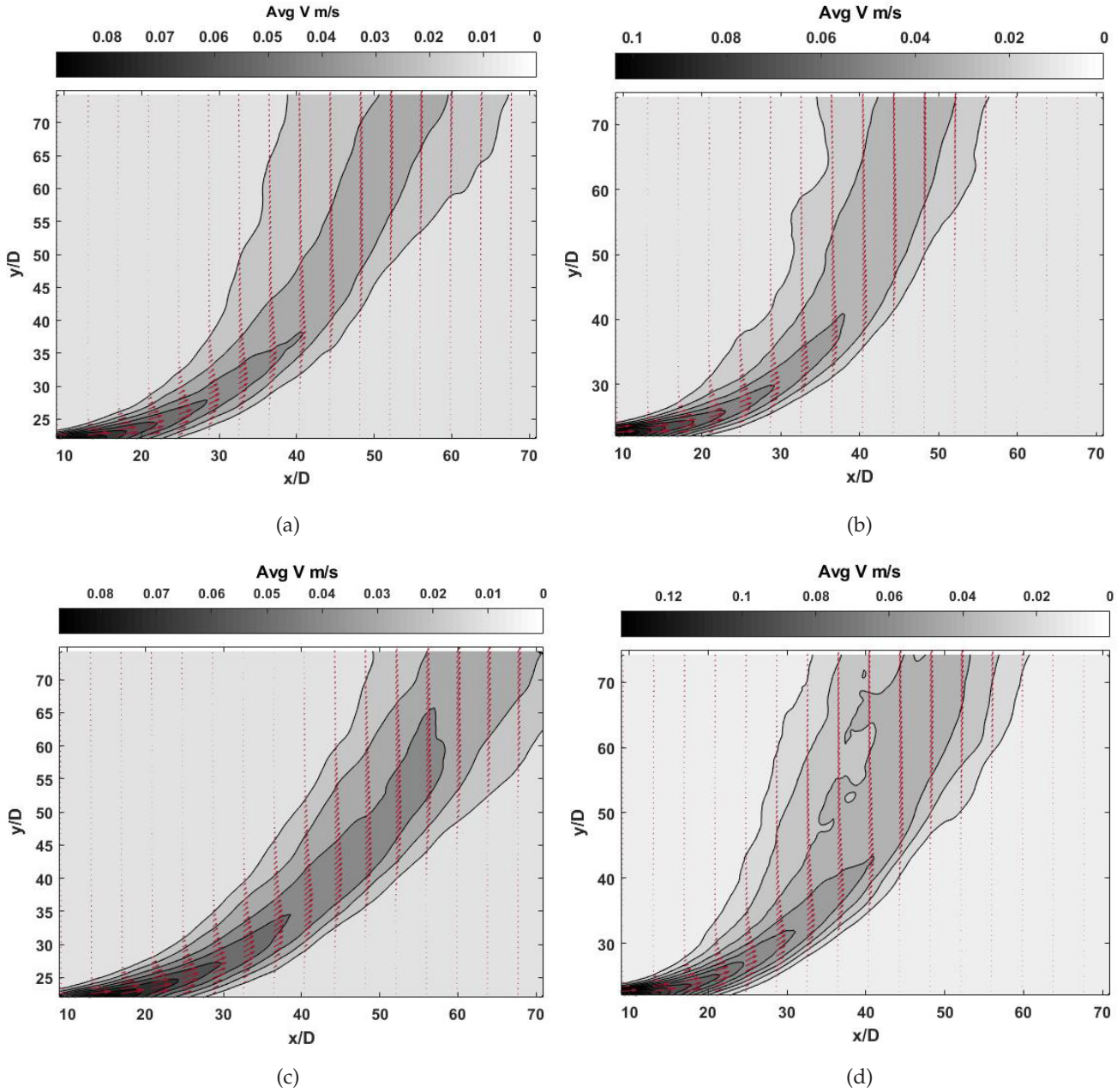

Fig. 5. Dimensionless mean velocity vectors with contour maps for: (a) case T1- thermal jet; (b) case S1- nonthermal jet; (c) case T3- thermal jet; and (d) case S3- nonthermal jet.

in the behavior of the jet trajectory between the two sets of experiments. As shown in these figures, all nonthermal jets were above the thermal jets, indicating that in the dense water, the nonthermal jets rose toward the water surface more rapidly and within a shorter distance from the nozzle than did the thermal jets. Although the values of Δρ and Fr_d were equal between the experiments in all comparisons, it can be seen that the nonthermal jets behaved differently than the thermal jets.

In addition, an effect of Δρ was clearly observed on jet trajectory behavior. The deviation between the thermal and nonthermal jet centerlines due to Δρ increased even though the values of Fr_d were equal (Figs. 6a and b). Moreover, Fr_d had an almost nonexistent effect, although the value was changed, while Δρ values remained almost the same (Figs. 6b and c). As a result, one can conclude that differences in density can affect jet trajectory behavior; therefore, salinity can play an important role in jet flow. In other words, the reason underlying the density difference (i.e., of thermal or nonthermal origin) could be a significant factor in the way in which the jet mixes with the ambient water.

4.5. Cross-sectional velocity profile

When studying buoyant jets, the velocity and concentration distributions at the cross-sections are often com-

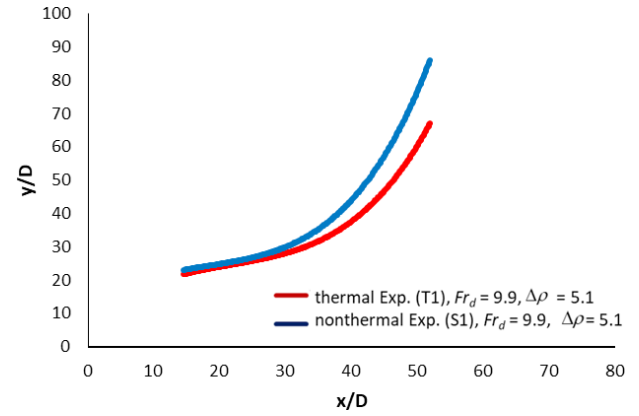

(a)

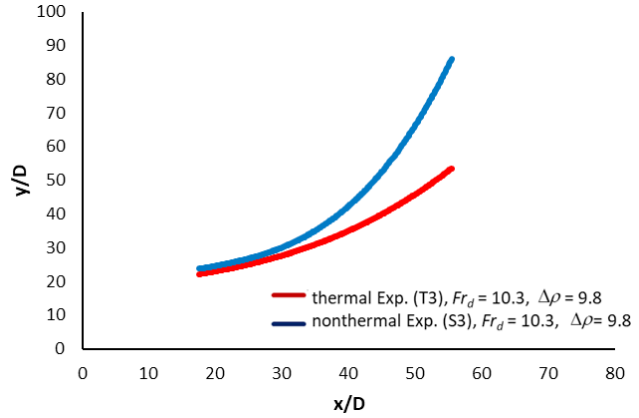

(b)

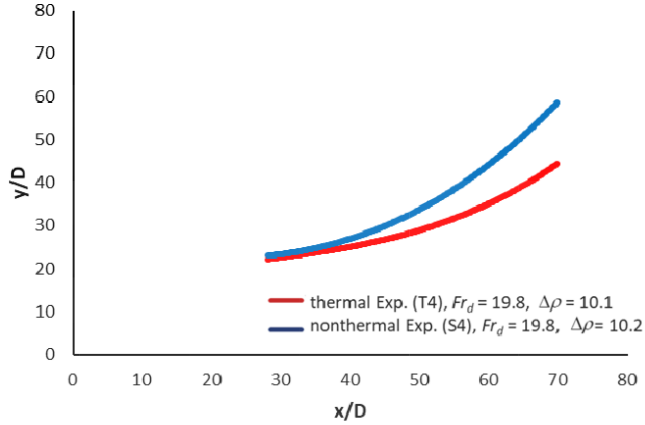

(c)

Fig. 6. Centerline trajectory of the velocity profile for both experiments: (a) comparison of T1 with S1; (b) comparison of T3 with S3; and (c) comparison of T4 with S4.

pared with the Gaussian profile. This comparison is valid when the jet has entered a region known as the zone of established flow (ZEF) [34]. In the present study, various cross-sectional profiles were selected along the axial centerline velocity of the jet for each experiment.

Fig. 7 illustrates the normalized cross-sectional profiles of U/U_m against r/b at various downstream locations, where r is the radial distance, and b is the distance from the point of maximum velocity (centerline) to the point where the velocity decreases and is equal to $1/e = 0.37$. As mentioned previously, for brevity, only the results of two comparative experiments (T1 with S1 and T3 with S3) are shown (Fig. 7). The extracted cross-sectional profiles were recorded at the same distance from the source of the jet (nozzle) for T1 and S1 (s/D = 6, 10, 14, 23, 31, 37 and 47) and for T3 and S3 (s/D = 3, 7, 11, 16, 22, 27 and 50). These profiles were then compared with a typical Gaussian profile to evaluate the distribution and evolution of the jet pattern. In general, the selected profiles for all experiments follow a Gaussian distribution and show a well-developed axisymmetric profile.

A reasonable Gaussian distribution is seen for the outer (lower) half of the various cross-sections for both experiments. However, it was observed that the comparison of T3 and S3 (Figs. 7c,d) better fitted a Gaussian distribution. Additionally,in both comparison cases, it can be seen that as the jet gets farther from the source (the nozzle), the inner (upper) half spreads out more widely and gradually diverges from the jet centerline. This phenomenon is observed clearly in the nonthermal cases and is mainly attributed to buoyancy-induced distortions, which can be seen in the inner (lower) half of the dense jet [22]. This distortion appears to increase with increased distance from the source to the water surface. When comparing the distributions of the thermal and nonthermal jets, the results reveal that the inner half distribution spreads farther for the nonthermal jets than for the thermal jets. As a result, nonthermal jets can decay and rise toward the water surface more rapidly than thermal jets; this result is consistent with the findings of Rathore and Das [31], in which the thermal energy of the jet is lost in the surrounding fluid due to the latter's coldness.

4.6. Jet growth rate

Jet width is commonly used to characterize jet growth rate. This is based on the Gaussian profile for various cross-sections of axial velocity distribution along the jet centerline. The growth rates of the velocity half-widths are calculated by plotting the nondimensionless values of b/D against the distances of the streamwise cross-section (s/D) along the jet centerline from the nozzle tip. The outer and inner half-widths of both jets are combined in the same figure to clearly show the difference in the spread widths, as seen in Fig. 8. The upper spread widths show more scatter than the lower spread widths, especially for the thermal jet. As shown in the figure, the tendency of both jets to spread is revealed when moving downstream and away from the nozzle, along the jet trajectory. After a short distance from the nozzle, the inner (upper) width of the thermal jet deviates and spread more than of the non thermal jet. As mentioned previously, this result offers further evidence that thermal jets tend to be flatter and spread more, while nonthermal jets tend to rise more steeply. As a result, the jet width profiles provide good evidence that the nonthermal jets decrease in intensity more rapidly as the flow turns toward the water surface over a shorter distance, and thus a shorter time exists for spreading and dilution.

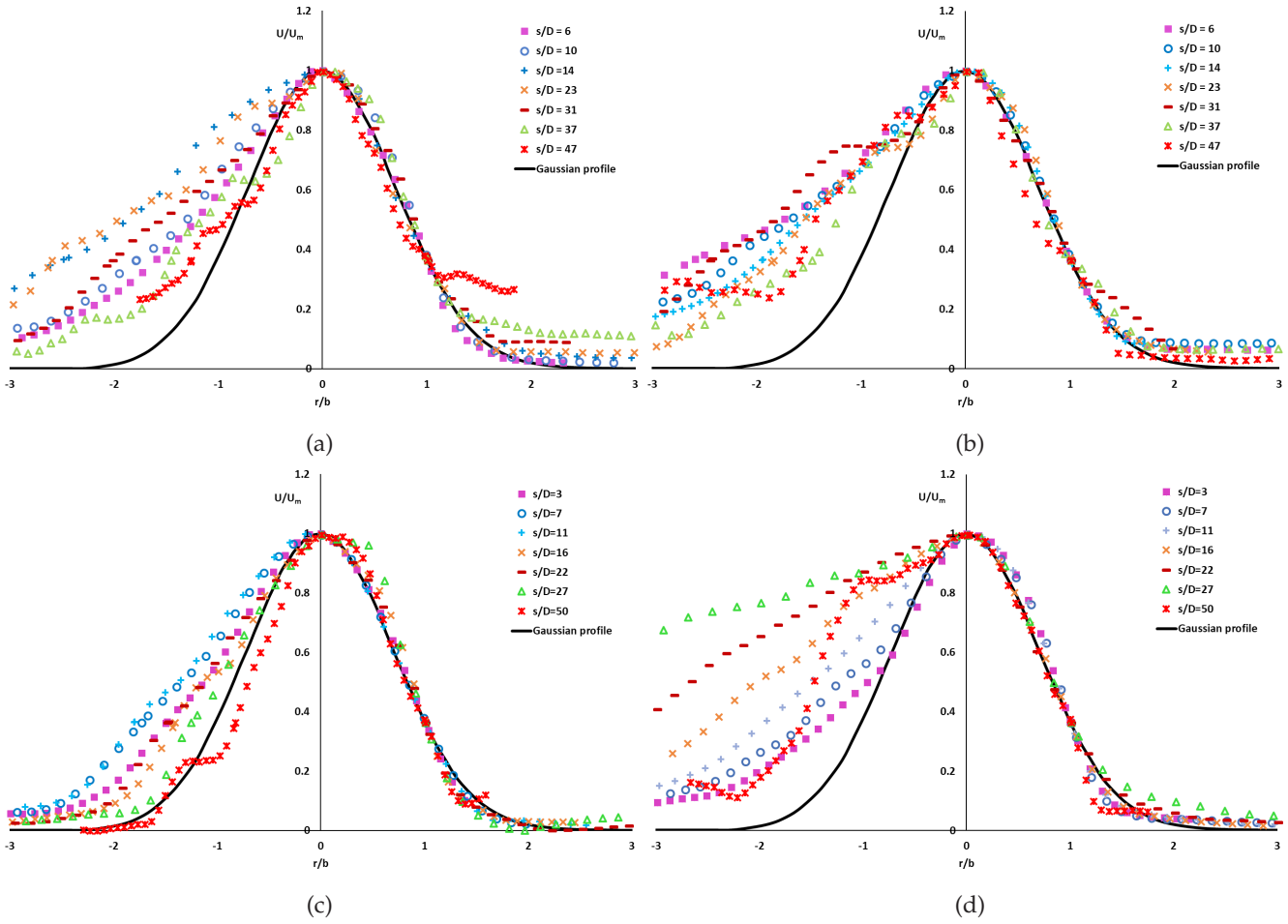

Fig. 7. Nondimensional velocity distribution profile at various downstream cross-sections along the jet centerline for: (a) thermal jet for case T1; (b) nonthermal jet for case S1; (c) thermal jet for case T3; and (d) nonthermal jet for case S3.

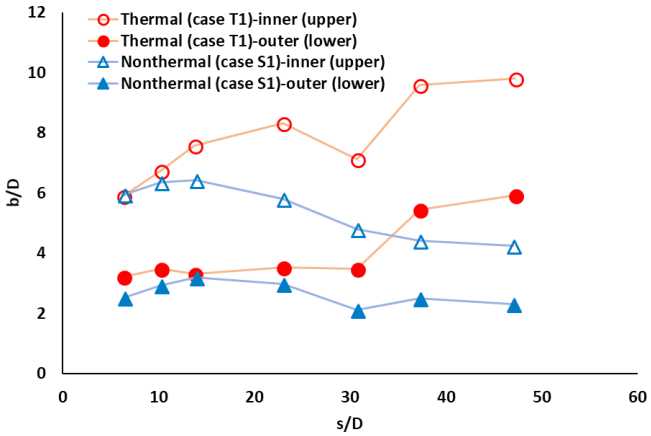

Fig. 8. Comparison between the velocity spread widths along the jet trajectory for thermal and nonthermal jets for cases T1 and S1.

4.7. Streamwise velocity decay

To further illustrate the effect of the receiving water conditions on the two buoyant offset jet flows (thermal and nonthermal) having similar properties, the results for the jet streamwise velocity decay are also presented. The U_m at several cross-sections of the jet centerline are extracted and plotted against the downstream of the jet source for four selected cases (comparing T1 with S1 and T3 with S3), as shown in Fig. 9.

Fig. 9a compares the velocity decays for T1 and S1 at a difference in density of approximately 5 kg/m^3. Both the thermal and nonthermal velocity decays closely follow those of the pure jet with a value of 7 for the constant K from Eq. (1), which is consistent with results reported in the literature [25,35]. Another comparison of decays having a higher difference in density of approximately 10 kg/m^3 is shown in Fig. 9b. In this figure, both the thermal and nonthermal maximum velocities decayed faster than those of the pure jet, and the divergence between the velocity values for both cases and those of the pure jet is obvious. In this case, the value of K was found to be 6.55 and 6.62 for the thermal and nonthermal jets, respectively. Although these values are almost identical, it is noted that a difference in density can affect a jet by accelerating its decay. In the case of a dense jet, two factors can affect the velocity decay: jet spreading and negative buoyancy [36]. Accordingly, an offset buoyant jet can also be affected by jet spreading and positive buoyancy. However, based on the present results, we find that a difference in density between a jet and the receiving water represents another significant factor that can accelerate jet decay.

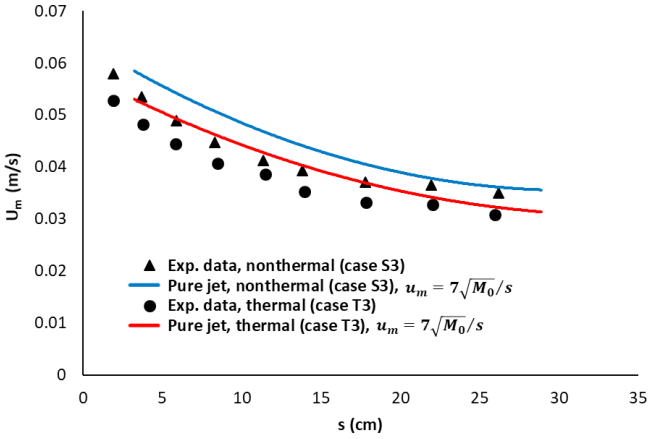

(a)

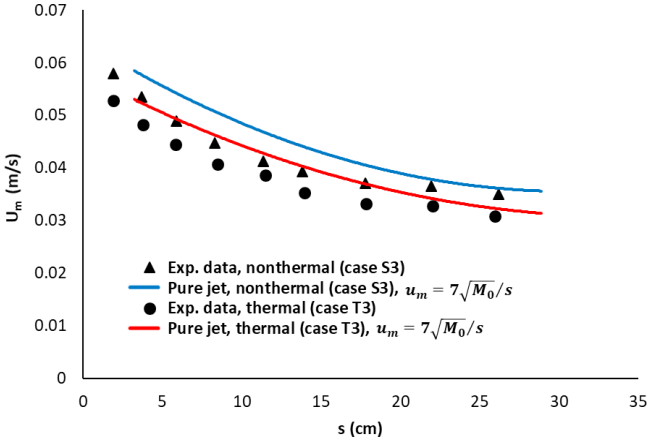

(b)

Fig. 9. Streamwise velocity decay of thermal and nonthermal jets compared with a pure jet: (a) cases T1 and S1, and (b) cases T3 and S3.

5. Computational approach

5.1. Governing equations

Three-dimensional turbulent flow of the RANS equations are used as the governing equations for incompressible fluids as follows:

Continuity equations:

$$\frac{\partial u_x}{\partial x}+\frac{\partial u_y}{\partial y}+\frac{\partial u_z}{\partial z}=0 \tag{2}$$

Momentum equations:

$$\frac{\partial u_x}{\partial t}+\frac{u_x\partial u_x}{\partial x}+\frac{u_y\partial u_x}{\partial y}+\frac{u_z\partial u_x}{\partial z}=\frac{\partial}{\partial x}\left[v_e\left(\frac{\partial u_x}{\partial x}\right)\right]+\frac{\partial}{\partial y}\left[v_e\left(\frac{\partial u_x}{\partial y}\right)\right]+\frac{\partial}{\partial z}\left[v_e\left(\frac{\partial u_x}{\partial z}\right)\right]-\frac{1}{\rho_0}\frac{\partial P}{\partial x} \tag{3}$$

$$\frac{\partial u_y}{\partial t}+\frac{u_x\partial u_y}{\partial x}+\frac{u_y\partial u_y}{\partial y}+\frac{u_z\partial u_y}{\partial z}=\frac{\partial}{\partial x}\left[v_e\left(\frac{\partial u_y}{\partial x}\right)\right]+\frac{\partial}{\partial y}\left[v_e\left(\frac{\partial u_y}{\partial y}\right)\right]+\frac{\partial}{\partial z}\left[v_e\left(\frac{\partial u_y}{\partial z}\right)\right]-\frac{1}{\rho_0}\frac{\partial P}{\partial y}-g' \tag{4}$$

$$\frac{\partial u_z}{\partial t}+\frac{u_x\partial u_z}{\partial x}+\frac{u_y\partial u_z}{\partial y}+\frac{u_z\partial u_z}{\partial z}=\frac{\partial}{\partial x}\left[v_e\left(\frac{\partial u_z}{\partial x}\right)\right]+\frac{\partial}{\partial y}\left[v_e\left(\frac{\partial u_z}{\partial y}\right)\right]+\frac{\partial}{\partial z}\left[v_e\left(\frac{\partial u_z}{\partial z}\right)\right]-\frac{1}{\rho_0}\frac{\partial P}{\partial z} \tag{5}$$

where u_x, u_y and u_z are the components of the mean velocity in the Cartesian coordinates; P is the fluid pressure; t is the time; v_e is the effective kinematic viscosity of water ($v_e = v_t + v$); v_t is the turbulent kinematic viscosity; and v is the kinematic viscosity. The effect of variable density (buoyancy) in the vertical direction (y-coordinate) is considered and added in Eq. (4).

Temperature and Salinity Equations:

$$\frac{\partial T}{\partial t}+\frac{u_x\partial T}{\partial x}+\frac{u_yT}{\partial y}+\frac{u_zT}{\partial z}=k_e\frac{\partial}{\partial x}\left[\frac{\partial T}{\partial x}\right]+\frac{\partial}{\partial y}\left[\frac{\partial T}{\partial y}\right]+\frac{\partial}{\partial z}\left[\frac{\partial T}{\partial z}\right] \tag{6}$$

$$\frac{\partial S}{\partial t}+\frac{u_x\partial S}{\partial x}+\frac{u_yS}{\partial y}+\frac{u_zS}{\partial z}=k_e\frac{\partial}{\partial x}\left[\frac{\partial S}{\partial x}\right]+\frac{\partial}{\partial y}\left[\frac{\partial S}{\partial y}\right]+\frac{\partial}{\partial z}\left[\frac{\partial S}{\partial z}\right] \tag{7}$$

where:

$$k_e=\frac{v_t}{\mathrm{Pr}_t}+\frac{v}{\mathrm{Pr}} \tag{8}$$

where k_e is the heat transfer coefficient, Pr is the Prandtl number, and Pr_t is the turbulent Prandtl number. The common ranges of both Pr and Pr_t are 0.6–1.0; both parameters are chosen as 1.0 based on Kheirkhah Gildeh et al. [22,37,38]. The details of the buoyancy-modified k-ε turbulence model are not described here for brevity but can be found in Yan and Mohammadian [39].

5.2. Boundary conditions

In the present study, only half of the buoyant offset jet domain is considered because of the symmetrical nature of the problem. Figs. 10a, b illustrate the computational domain with the mesh system. The dimensions of the computational domain (Fig. 10a) were chosen to simulate the present experiments. A refined mesh is considered in the near-field area of the offset jet for all simulations to better capture the velocity and temperature characteristics, as shown in Fig. 10b. The parameters used herein are similar to those used in the experiments (see Table 1). The nozzle boundary conditions are chosen based on Kheirkhah Gildeh et al. [37,38] as follows: $u_x = U_0$, $u_y = u_z = 0$, $T = T_0$, $k = 0.06u^2$, $\varepsilon = 0.06u^3/D$. A zero gradient boundary condition perpendicular to the outlet plane is defined for u_x, u_y, u_z, k, ε, T, and S for the flow at the outlet boundary section. For the walls, boundary conditions defined as z and $u_z = 0$ and a no-slip condition were applied in this study. Thus, k and ε are assumed to follow standard wall functions at the wall for both thermal and nonthermal buoyant jets. Finally, the symmetry boundary was modeled using a symmetry plane condition.

5.3. Numerical simulation

In this study, the finite volume open source code OpenFOAM with a structured grid was used to simulate buoyant offset jet discharge. The OpenFOAM [24] (a free

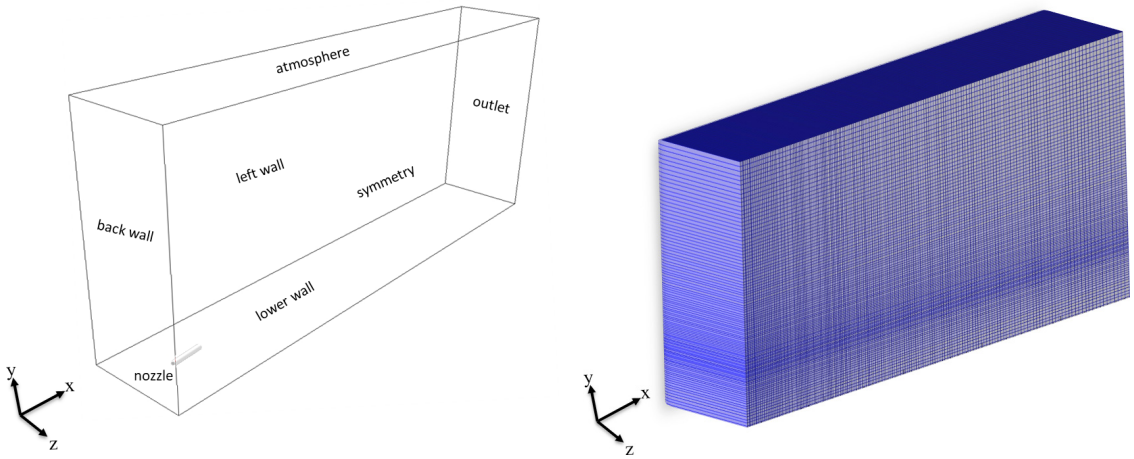

Fig. 10. Computational domain: (a) The numerical model domain and boundary definitions; and (b) the structured grid of the domain with a refined mesh near the nozzle.

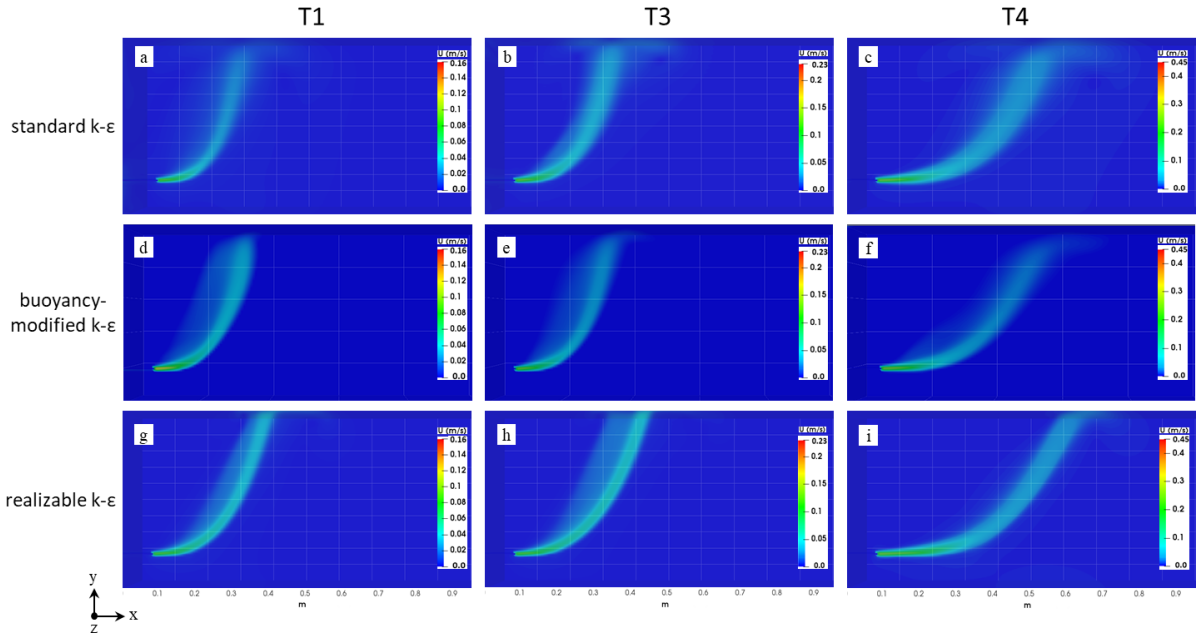

Fig. 11. Jet behavior according to the numerical simulation results: (a, b and c) the standard *k*-ε model; (d, e and f) the buoyancy-modified *k*-ε model; and (g, h and i) the realizable *k*-ε model.

open-source package) is widely used for modeling and solving scientific problems, including positively and negatively buoyant jets [23,37,38]. The model solves a set of partial differential equations (PDEs) using the finite volume method (FVM). The base pisoFoam solver for incompressible fluids was developed for use in this study. The advection-diffusion equation for salinity and temperature was added to calculate the transport and dispersion of these parameters. Three RANS turbulence models were chosen for this study due to their better accuracy compared with other RANS turbulence models, as reported in recent studies by Kheirkhah Gildeh et al. [22,37,38] and Yan and Mohammadian[39]. These models are the standard *k*-ε, realizable *k*-ε and buoyancy-modified *k*-ε models.

5.4. Numerical results

5.4.1. Comparison with experimental results

In this section, the preliminary results of the numerical simulation are compared with various experimental data presented in this study. The experimental results of six thermal and nonthermal cases (T1, T3, T4 and S1, S3, S4) were selected to examine the performance of three turbulence models (the standard *k*-ε, realizable *k*-ε, and buoyancy-modified *k*-ε models) under the same conditions. The general behavior of the jets according to the numerical results for all models and the disparities between the results (cases 1, 2 and T3) can be observed in Fig. 11.

Fig. 12 shows the numerical results of the centerline trajectory for all models and compares them with the experimental results. The comparison shows that the numerical results obtained for all models were in good agreement with cases T4 and S4. More comparison between the data extracted from the PIV measurements and the models tested here can be shown in Fig. 13. In this figure, the velocity field contours of the numerical results are compared with experimental results (cases T1 and S1). As shown in this figure, the realizable *k*-ε model predicts better, but thinner when compared to the experimental contours. This was clearly seen in all results of the numerical models. This could be due to the isotropic assumption of these turbulence models, as a Linear Eddy Viscosity Models (LEVMs), where the jet predicted by these models is usually thinner [38].

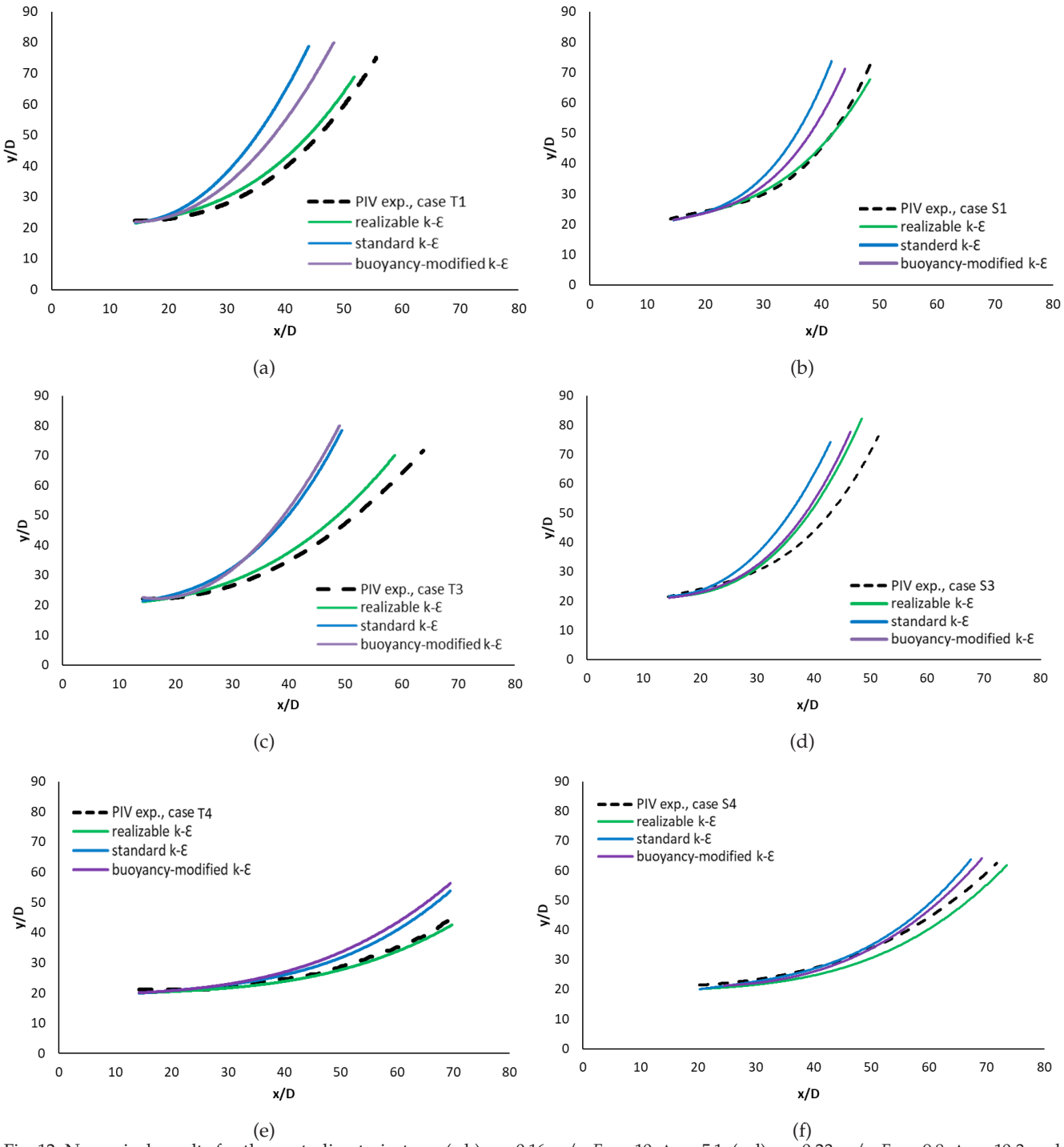

Fig. 12. Numerical results for the centerline trajectory: (a,b) u = 0.16 m/s, Fr_d = 10, Δρ = 5.1; (c,d) u = 0.23 m/s, Fr_d = 9.8, Δρ = 10.3 and (e,f) u = 0.45 m/s, Fr_d = 19.8, Δρ = 10.1.

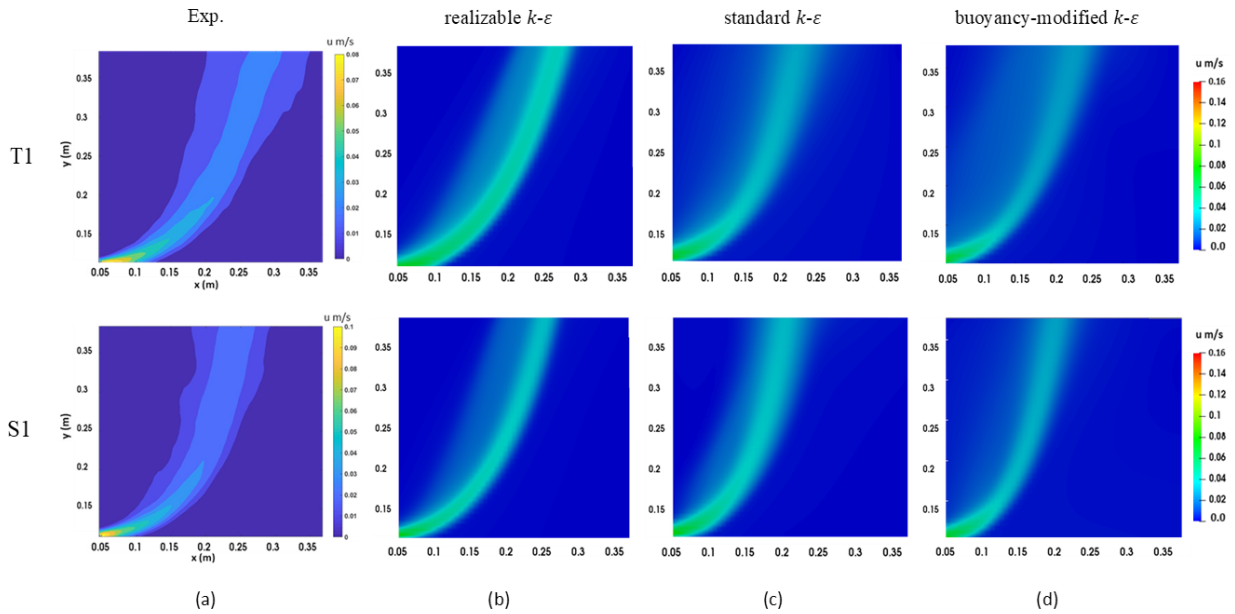

Fig. 13. Comparison of the velocity field contours: (a) the experimental result of the case T1 and S1; (b) the realizable *k*-ε model; (c) the standard *k*-ε model; and (d) the buoyancy-modified *k*-ε model.

In addition, a good match was observed between the numerical results obtained using the realizable *k*-ε model and all other experimental cases, except S3. As mentioned, one can see clearly from the figures that the realizable *k*-ε model better predicts the results than the standard *k*-ε and buoyancy-modified *k*-ε turbulence models. This can be attributed to the different calculations of eddy viscosity (v_t) in the *k*-ε turbulence models which make the results different. This is due to the difference in the calculation of the Cμ for these models, which is non-constant value in the realizable *k*-ε while a constant value for others (0.09). Thus, the outcome from the v_t will change and give a different result comparing to standard *k*-ε and buoyancy-modified *k*-ε models. As a result, the realizable *k*-ε provides a more accurate prediction.

Moreover, the standard *k*-ε and buoyancy-modified *k*-ε models better predict the results for cases T4 and S4 than for other cases in which the value of Fr_d is increased. Accordingly, the standard *k*-ε and the buoyancy-modified *k*-ε models can good predictions in cases where the value of the Fr_d is high.

Consequently, the numerical results of the realizable *k*-ε model are in good agreement with all experimental cases presented in this study. More results and details of various numerical models compared with the present experimental data are currently being by the authors.

To quantify the variations in the centerlines of the turbulence models with the centerlines of the experimental cases, values of the Standard Error of the Estimate (SEE) were calculated for all turbulence models using the following equation:

$$SEE = \sqrt{\Sigma(\hat{y} - y)^2 / n} \tag{9}$$

where ŷ is the estimated (numerical) value, y is the experimental value, and n is the number of observations. The results for all turbulence models are summarized in Table 2. The values of the standard error of the estimate show that the realizable *k*-ε model is the most preferred model. In addition, the results show that the buoyancy-modified *k*-ε provided better prediction than the standard *k*-ε in all nonthermal cases, and was the best for the case S4.

Table 2
Values of the standard error of the estimate for the comparison of the centerline trajectories of the tested turbulence models with the experimental results

Case	Turbulence model		
	Standard k-ε	Realizable k-ε	Buoyancy-modified k-ε
T1	17.27	2.99	12.64
T3	13.85	2.60	15.20
T4	3.84	0.96	5.25
S1	6.58	0.77	4.15
S3	6.15	3.91	4.38
S4	1.10	1.51	0.82

6. Conclusion

This paper presents the results of an experimental study of thermal and nonthermal buoyant offset jets discharged into fresh and saline ambient waters. The influence of the ambient water conditions on jet behavior was the focus of this study. Therefore, the characteristics of a jet affected by changes in the properties of the ambient water have been investigated in detail, including jet propagation, patterns, centerline trajectory, and jet width and decay. Fourteen cases (7 thermal and 7 nonthermal) have been considered in this study. In the first set of cases (thermal experiments),

a density gradient was caused by difference in temperature only, whereas salinity was assumed to be constant (i.e., zero). In the second set of experiments (nonthermal cases), the density gradient was caused by salinity and the domain temperature was constant. The Fr_d and Δρ were kept similar for all comparative experiments. As a controlling parameter, this consideration was applied in the present study to determine whether the source of the density difference (temperature versus salinity) can affect jet behavior. In general, the results show that jet flows behave differently if discharged into ambient water with different conditions. It was also observed that the jets rose in the saline ambient (i.e., nonthermal) cases faster than in the fresh ambient (thermal) cases. The propagation speed was shown to be slower, and the time taken to reach the surface was longer for the thermal jets, while the nonthermal jets propagated more rapidly and reached the surface in less time and over shorter distances. The results showed that thermal jets had different patterns due to their slower motion and longer distance to reach the water surface when compared with the nonthermal jets. Differences in the trajectories between the thermal and nonthermal jets were clearly noted, even though the Fr_d and the Δρ remained the same. Therefore, it is concluded that the Fr_d and the Δρ cannot be the only controlling factors in jet evolution. In addition, based on the jet growth and velocity decay rates, the nonthermal jets decayed faster than the thermal jets in all the experiments.

Moreover, three RANS turbulence models, (the standard *k*-ε , realizable *k*-ε and buoyancy-modified *k*-ε models) were applied to predict the behavior of these jets. The numerical results for the jet trajectory obtained using the realizable *k*-ε model was in good agreement with all experimental data. Finally, the buoyancy-modified *k*-ε model better predicted jet trajectory than the standard *k*-ε turbulence model, especially in the nonthermal cases. Further investigations into buoyant offset jets with higher Froude numbers and various numerical models is currently in progress by the authors. In conclusion, this study demonstrates that ambient water conditions can significantly affect jet characteristics and behaviors.

Acknowledgments

Hassan Alfaifi would like to acknowledge King Abdulaziz City for Science and Technology (KACST) for financial support during his PhD study. The research was partially supported by the Natural Sciences and Engineering Research Council of Canada (NSERC).

Symbols

Fr_d — Densimetric Froude number
Δρ — Density differences
U — Jet velocity
U_a — Ambient water velocity
$U_m = u_m$ — Mean velocity of the jet centerline
U_0 — Initial jet velocity
D — Jet diameter
ρ_a — Ambient water density
ρ_0 — Initial jet density
s — The streamwise coordinates of the jet
B — Jet half-width, the distance from the point of maximum velocity (centerline) to the point where the velocity decreases to $1/e = 0.37U_m$
M_0 — Momentum flux
B_0 — Buoyancy flux
Q_0 — Discharge volume
g' — Effective gravitational acceleration
g — Gravitational acceleration
L_M — Momentum length scale
L_Q — Source length scale
K — A constant, can be obtained experimentally
T — Temperature
S — Salinity
S_A — Absolute salinity
T_0 — Initial temperature
T_a — Ambient water temperature
S_0 — Initial salinity
S_a — Ambient water salinity
$\Delta\rho_{thermal}$ — Density differences due to temperature
$\Delta\rho_{nonthermal}$ — Density differences due to salinity
t — Time
r — Radial distance
u_x, u_y, u_z — Components of the mean velocity in the cartesian coordinates
P — Fluid pressure
Pr — Prandtl number
Pr_t — Turbulent Prandtl number

Greek

v_e — Effective kinematic viscosity of water ($v_e = v_t + v$)
v_t — Turbulent kinematic viscosity
v — Kinematic viscosity
k_e — Heat transfer coefficient
k — Turbulent kinetic energy
ε — Turbulent dissipation rate

References

[1] M. Ahmad, Environmental effects of multi-stage flash (MSF) desalination plant at Al Jubail, Saudi Arabia, master dissertation, Memorial university of Newfoundland, Newfoundland, Canada, 2002.
[2] B. Mabrook, Environmental impact of waste brine disposal of desalination Plants, Red Sea, Egypt, Desalination, 97 (1994) 453–465.
[3] A. Hashim, M. Hajjaj, Impact of desalination plants fluid effluents on the integrity of seawater, with the Arabian gulf in perspective, Desalination, 182 (2005) 373–393.
[4] S.Lattemann, T. Höpner, Environmental impact and impact assessment of seawater desalination, Desalination, 220 (2008) 1–15.
[5] M. Milione, C. Zeng, The effects of temperature and salinity on population growth and egg hatching success of the tropical calanoid copepod, AcartiaSinjiensis, Aquaculture, 275 (2008) 116–123.
[6] D.A. Roberts, E.L. Johnston, N.A. Knott, Impacts of desalination plant discharges on the marine environment: a critical review of published studies, Water Res., 44 (2010) 5117–5128.
[7] M.L. Cambridge, A. Zavala-Perez, G.R. Cawthray, J. Mondon, G.A. Kendrick, Effects of high salinity from desalination brine on growth, photosynthesis, water relations and osmolyte concentrations of seagrass Posidonia australis, Marine Pollut. Bull., 115 (2017) 252–260.

[8] C.H. Bosanquet, G. Horn, M.W. Thring, The effect of density differences on the path of jets, Proc. R. Soc. Lond. A, 263 (1961) 340–352.
[9] J. Hoch, L.M. Jiji, Two-dimensional turbulent offset jet-boundary interaction, J. Fluids Eng., 103 (1981) 154–161.
[10] R. Gu, Modeling two-dimensional turbulent offset jets, J. Hydraulic Eng., 122 (1996) 617–624.
[11] A. Nasr, J.C.S. Lai, A turbulent plane offset jet with small offset ratio, Exp. Fluids, 24 (1998) 47–57.
[12] P.R. Rajesh Kanna, M.K. Das, Numerical simulation of two-dimensional laminar incompressible offset jet flows, Int. J. Numer. Meth. Fluids, 49 (2005) 439–464.
[13] D. Shao, A.W.K. Law, Turbulent mass and momentum transport of a circular offset dense jet, J. Turbulence, 10 (2009) 1–24.
[14] D. Shao, A.W.K. Law, Boundary impingement and attachment of horizontal offset dense jets, J. Hydroenviron. Res., 5 (2011) 15–24.
[15] M. Agelin-Chaab, M.F. Tachie, Characteristics of turbulent three-dimensional offset jets, J. Fluids Eng., 133(5) (2011) 051203.
[16] A. Assoudi, S. Habli, N.M. Saïd, H. Bournot, G. Le Palec, Experimental and numerical study of an offset jet with different velocity and offset ratios, Eng. Appl. Comput. Fluid Mech., 9 (2015a) 490–512.
[17] A. Assoudi, S. Habli, N.M. Saïd, H. Bournot, G. Le Palec, Three-dimensional study of turbulent flow characteristics of an offset plane jet with variable density, Heat Mass Trans., 52(11) (2016) 2327–2343.
[18] A.M. Rawn, H.K. Palmer, Predetermining the extent of a sewage field in sea water, Trans. Am. Soc. Civil Eng., 94 (1930) 1036–1060.
[19] S.N. Michas, P.N. Papanicolaou, Horizontal round heated jets into calm uniform ambient, Desalination, 248 (2009) 803–815.
[20] O. Eleuch, N. Latrache, S. Frikha, Z. Driss, Experimental study of the injection of a pure water jet in miscible salt water, Thermo-Mechanics Applications and Engineering Technology, Springer, Cham, 2018, pp. 223–241.
[21] P. Liu, K.M. Lam, Large-eddy simulation of horizontally discharging sediment-laden jets, J. Hydroenviron. Res., 9 (2015) 388–403.
[22] H. Kheirkhah Gildeh, A. Mohammadian, I. Nistor, H. Qiblawey, Numerical modeling of turbulent buoyant wall jets in stationary ambient water, J. Hydraul Eng., 140(6) (2014) 04014012.
[23] S. Zhang, B. Jiang, A.W.K. Law, B. Zhao, Large eddy simulations of 45° inclined dense jets, Environ. Fluid Mech., 16 (2016) 101–121.
[24] OpenFOAM version 5 [Computer software]. User guide, OpenCFD Limited, 2017.
[25] H.B. Fischer, E.J. List, R.C.Y. Koh, J. Imberger, N.H. Brooks, Mixing in inland and coastal waters. Academic Press, San Diego, 1979.
[26] A.J.S. Cuthbertson, P.A. Davies, Deposition from particle-laden, round, turbulent, horizontal, buoyant jets in stationary and coflowing receiving fluids, J. Hydraul. Eng., 134 (2008) 390–402.
[27] F.J Millero, A. Poisson, International one-atmosphere equation of state of seawater, Deep Sea Research Part A, Oceanographic Research Papers, 28(6) (1981) 625–629.
[28] F.J. Millero, F. Huang, The density of seawater as a function of salinity (5 to 70 g/kg) and temperature (273.15 to 363.15 K), Ocean Sci., 5(2) (2009) 91–100.
[29] M. Raffel, C. Willert, S. Wereley, J. Kompenhans, Particle image velocimetry, a practical guide, second ed., Springer-Verlag, Berlin, 2007.
[30] H. Alfaifi, A. Mohammadian, H. Kheirkhah Gildeh, Comparison of salinity and temperature mixing: experimental and numerical study, in: Proceedings of the International Symposium on Outfall Systems, ISOS 2016, IAHR-IWA joint committee on marine outfall systems, Ottawa, Canada.
[31] S.K. Rathore, M.K. Das, A comparative study of heat transfer characteristics of wall-bounded jets using different turbulence models, Int. J. Therm. Sci., 89 (2015) 337–356.
[32] P.J.W. Roberts, G. Toms, Inclined dense jets in flowing current, J. Hydraulic Eng., 113 (1987) 323–340.
[33] M.A. Zeitoun, W.F. McIlhenny, Conceptual designs of outfall systems for desalination plants, in: Proceedings of the Offshore Technology Conference, 1971.
[34] D. Shao, A.W.K. Law, Mixing and boundary interactions of 30° and 45° inclined dense jets, Environ. Fluid Mech., 10 (2010) 521–553.
[35] J.H.W. Lee, V. Chu, Turbulent Jets and Plumes: a Lagrangian Approach, Kluwer Academic Publishers, Springer Science & Business Media New York, 2003.
[36] C.C.K. Lai, J.H.W. Lee, Mixing of inclined dense jets in stationary ambient, J. Hydroenviron. Res., 6 (2012) 9–28.
[37] H. Kheirkhah Gildeh, A. Mohammadian, I. Nistor, H. Qiblawey, Numerical modeling of 30° and 45° inclined dense turbulent jets in stationary ambient, Environ. Fluid Mech., 15 (2015a) 537–562.
[38] H. Kheirkhah Gildeh, A. Mohammadian, I. Nistor, H. Qiblawey, X. Yan, CFD modeling and analysis of the behavior of 30 and 45 inclined dense jets-new numerical insights, J. Appl. Water Eng. Res., 4 (2015b) 1–16.
[39] X. Yan, A. Mohammadian, Numerical modeling of vertical buoyant jets subjected to lateral confinement, J. Hydraul. Eng., 143 (2017) 04017016.